

Learning Calibrated-Guidance for Object Detection in Aerial Images

Zongqi Wei[†], Dong Liang[†], Dong Zhang[†], Liyan Zhang^{*}, Qixiang Geng, Mingqiang Wei, *Senior Member, IEEE*, and Huiyu Zhou

Abstract—Object detection is one of the most fundamental yet challenging research topics in the domain of computer vision. Recently, the study on this topic in aerial images has made tremendous progress. However, complex background and worse imaging quality are obvious problems in aerial object detection. Most state-of-the-art approaches tend to develop elaborate attention mechanisms for the space-time feature calibrations with arduous computational complexity, while surprisingly ignoring the importance of feature calibrations in channel-wise. In this work, we propose a simple yet effective Calibrated-Guidance (CG) scheme to enhance channel communications in a feature transformer fashion, which can adaptively determine the calibration weights for each channel based on the global feature affinity correlations. Specifically, for a given set of feature maps, CG first computes the feature similarity between each channel and the remaining channels as the intermediary calibration guidance. Then, re-representing each channel by aggregating all the channels weighted together via the guidance operation. Our CG is a general module that can be plugged into any deep neural networks, which is named as CG-Net. To demonstrate its effectiveness and efficiency, extensive experiments are carried out on both oriented object detection task and horizontal object detection task in aerial images. Experimental results on two challenging benchmarks (*i.e.*, DOTA and HRSC2016) demonstrate that our CG-Net can achieve the new state-of-the-art performance in accuracy with a fair computational overhead. The source code has been open sourced at <https://github.com/WeiZongqi/CG-Net>

Index Terms—Attention learning, calibrated-guidance, object detection, aerial image, deep learning.

I. INTRODUCTION

OBJECT detection in aerial images is one of the most fundamental yet challenging research tasks, which aims to assign a bounding box with a unique semantic category label to each surficial object in the given aerial images [1]–[5]. This task is critical for a wide range of downstream tasks, *e.g.*, land resource management, ecological monitoring, and land ecosystem evaluation [6], [7]. Thanks to the recent promising development of deep Convolutional Neural Networks (CNNs) in image processing, object detection in aerial images has also

made tremendous progress. The state-of-the-art approaches are usually based on a one-stage detector (*e.g.*, RetinaNet [8] and YOLO [9]) or a two-stage detector (*e.g.*, Fast/Faster R-CNN [10], [11]) with a CNN as the backbone.

Compared to objects in general natural scenes, objects in aerial images usually have smaller size, higher density, objects with different size, worse imaging quality, and more complex background [12], [13]. Therefore, it is difficult to directly achieve a satisfying recognition performance in aerial images using the existing natural scene object detectors. To this end, state-of-the-art methods focus on developing effective head networks [1], adaptive dense anchor generators [2], and labeling strategy [3], [5]. Besides, effective feature learning strategies play a crucial role. Because such methods can provide generalized features to improve the model performance. To this end, a large amount of feature calibration methods based on the attention mechanisms have been proposed to improve the rough feature representations in CNNs [4], [6], [14]–[16]. Conceptually, these attention-based methods can be basically divided into two categories: (I) the spatial-attention-based one, and (II) the channel-attention-based one. For the first category (*e.g.*, spatial attention module [15]–[17], recurrent attention structure [6], self-attention mechanism [18], and non-local operation [19]), as shown in Figure 1 (a), a global context mapping for each feature position can be obtained by computing the similarities between the feature of each specific position and all the remaining feature positions [20]. Through such an operation, each pixel can obtain the long-range dependence information of the input image. For the second category (*e.g.*, channel attention module [17], and the channel-wise attention [15], [21], and the squeeze-and-excitation block [4], [14], [22]), as shown in Figure 1 (b), each channel can obtain a weight that reflects its own importance in object detection, and then integrate the weight into the model by the channel re-weighting manner.

Despite the success of the existing attention-based methods in calibrating features for object detection, we argue that most of these methods on feature calibrations in channels are not enough. That is to say, they cannot introduce channel communications to capture the dependencies between channel feature maps, which has empirically shown their benefits to a wide range of computer visual recognition tasks [25]–[30]. Although the existing channel-attention-based methods can enable different channels to obtain different weights, modules (*e.g.*, global average/max pooling) based on their channel feature maps cannot guarantee all the channels have sufficient communications. Therefore, from this point of view, these

Z. Wei, D. Liang, L. Zhang, Q. Geng, and M. Wei are with the College of Computer Science and Technology, Nanjing University of Aeronautics and Astronautics, MIIT Key Laboratory of Pattern Analysis and Machine Intelligence, Collaborative Innovation Center of Novel Software Technology and Industrialization, Nanjing 211106, China. E-mail: {weizongqi, liangdong, zhangliyan, gengqixiang, mqwei}@nuaa.edu.cn.

D. Zhang is with the School of Computer Science and Engineering, Nanjing University of Science and Technology, Nanjing 210094, China. E-mail: dongzhang@njust.edu.cn.

H. Zhou is with the School of Informatics, University of Leicester, Leicester LE1 7RH, United Kingdom. E-mail: hz143@leicester.ac.uk

[†] These authors contributed equally to this work.

^{*} Corresponding author: Liyan Zhang.

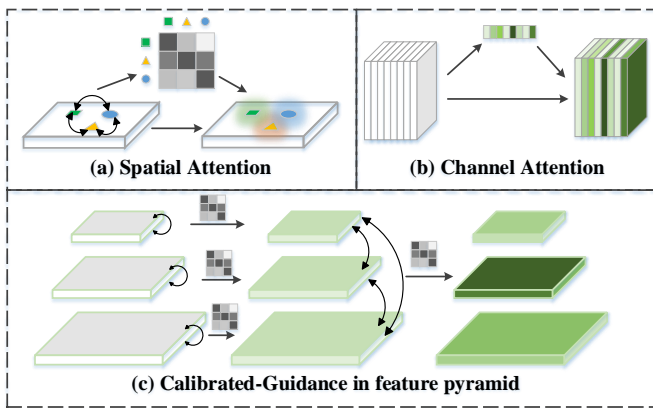


Fig. 1: Illustrations of the attention-based feature calibration methods, (a) spatial attention mechanism, (b) channel attention mechanism, and (c) our proposed calibrated-guidance.

methods are still local-based.

To address those problem, including different size objects and complex background in aerial images and limitations of existing attention-based methods in calibrating features, in this paper, we propose a simple yet effective Calibrated-Guidance (CG) scheme to enhance channel communications in a feature transformer fashion, which can adaptively determine the calibration weights for each feature channel based on the global feature affinity-pairs. CG is an active feature communication mechanism, as illustrated in Figure 1 (c), which can explicitly introduces feature dependencies in a channel-wise manner. Specifically, CG is applied to the pyramid features, including the inner and inter-layers of the pyramid, and the pyramid layer features are also regarded as the "channel" of overall pyramid features. CG consists of two steps: first, feature similarities (via the dot product operation) between each channel and the remaining channels are computed as the intermediary calibration guidance. Then, we represent each channel by aggregating all the channels weighted together via the guidance. The weighted feature maps has the same spatial size as the input feature maps, but contain richer information about the long-range channel dependency information. For typical problems of aerial images, within and between pyramid layers, we propose Base CG and Rearrange Pyramid CG to realize calibrating features locally and globally.

CG is a general unit that can be plugged into any deep neural network. We name a CNN model deployed the proposed CG module as CG-Net. The overall architecture is shown in Figure 2. To demonstrate its effectiveness and efficiency, we conduct extensive experiments on both oriented object detection task and horizontal object detection task. Experimental results on the challenging benchmarks DOTA [12] and HRSC2016 [31] for oriented object detection show that our proposed CG-Net can boost substantial improvements compared to the baseline methods and achieves the state-of-the-art performance in accuracy (*i.e.*, 77.89% and 90.58% mAP, respectively) with a fair computational overhead. Besides, experimental results on DOTA [12] for horizontal object detection also validate the flexibility and effectiveness of the

proposed CG-Net, which also achieves the new state-of-the-art performance with the accuracy by 78.26% mAP.

In summary, our main contributions are two-fold:

- a simple yet effective CG scheme is proposed to enhance channel communications in a feature transformer fashion, and implements within and between feature pyramid layer to enhance pyramid representation;
- we propose a CG-Net, which can achieve the state-of-the-art oriented and horizontal object detection performance on two challenging benchmarks for aerial images, including DOTA and HRSC2016.

II. RELATED WORK

A. Object Detection in Aerial Images.

The purpose of object detection in aerial images is to locate objects of interest on the ground and recognize their categories by a bounding box [13], [32]. Each bounding box not only contains the object coordinate information, but also contains the category information. Object detection in aerial images can be divided into horizontal-based ones and oriented-based ones. Horizontal object detection aims to detect objects with horizontal bounding boxes [8], [9], [11], [33]. Being observed from an overhead perspective, the objects in aerial images present more diversified orientations. Oriented object detection [1]–[5], [34]–[42] is an extension of horizontal object detection to accurately outline the objects, especially those with large aspect ratios.

Based on horizontal object detection, rotating boxes are important learning parts in oriented object detection. There are many methods on how to rotate boxes. CSL [3] design a detection frame by transforming angular prediction form a regression to a classification task. Gliding Vertex [36] glides the vertex of the horizontal bounding box (regressing four length ratios characterizing the relative gliding offset on each corresponding side) on each corresponding side to accurately describe a multi-oriented object. DAL [2] propose a dynamic anchor learning method, which utilizes the newly defined matching degree to comprehensively evaluate the localization potential of the anchors. RoI Trans [1] proposes a ROI Transformer to address the mismatches between the Region of Interests (RoIs) and objects on training. CFC-Net [38] proposes a Critical Feature Capturing Network to address problems of discriminative features in object detection in refining preset anchors, building powerful feature representation and optimizing label assignment. R-RPN [42] overcomes the limitation of ROI pooling when extracting ships features with various aspect ratios. For fast and accurate oriented object detection, R³Det [40] and O²-DNet [41] make attempts in one-stage model with RetinaNet and anchor free structures. Based on R³Det, R³Det-DCL [5] designs Densely Coded Labels (DCL) for angle classification, which replaces the Sparsely Coded Label (SCL) in classification-based detectors before, and reduces three times training speed, further bringing notable improvements in accuracy of detection tasks. What's more, for oriented object detection, SCRDet [4] combines pixel and channel attention network for small and cluttered objects.

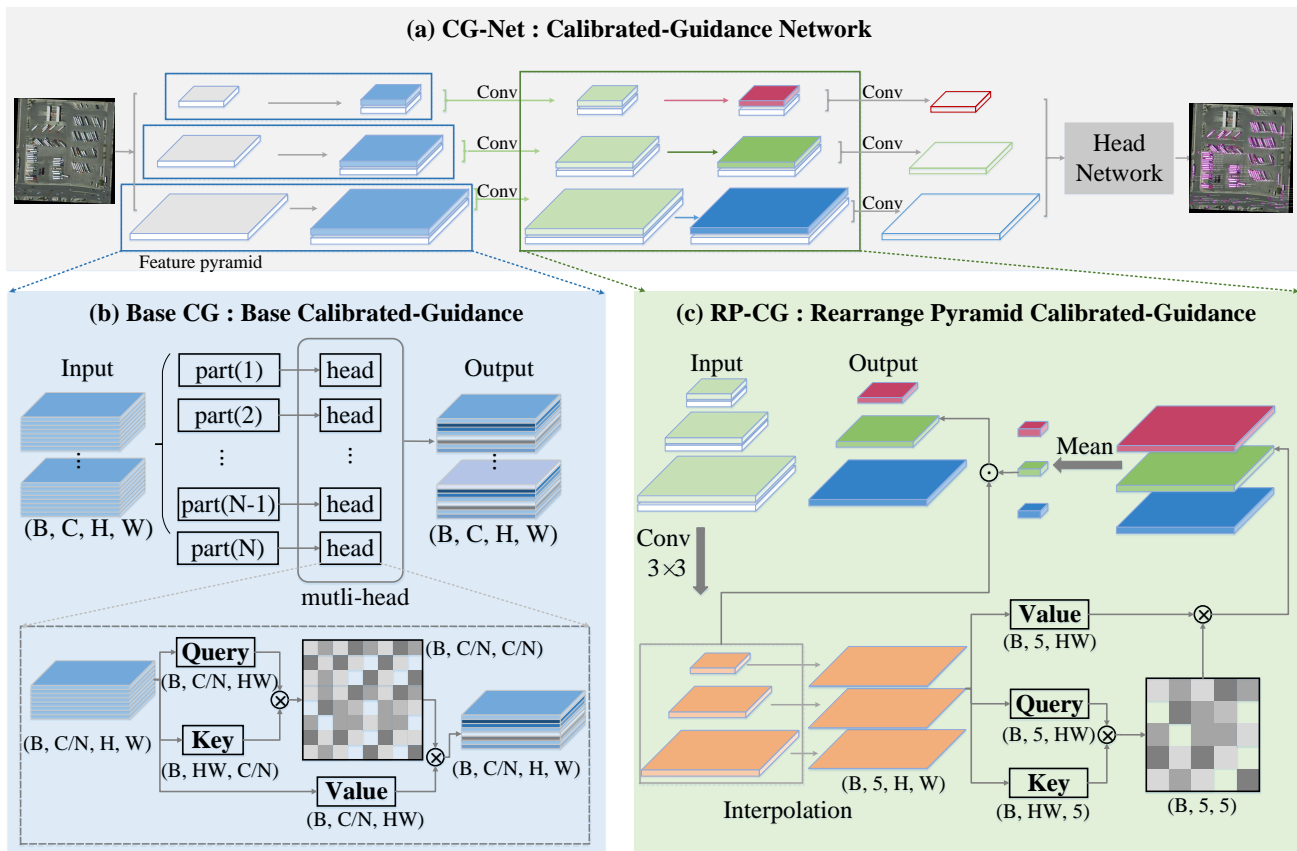


Fig. 2: Overall architecture of our proposed Calibrated-Guidance Network (CG-Net), where CG is deployed on both the intra-layer feature maps and the feature pyramid (*i.e.*, the standard feature pyramid network [23]). In comparison, feature map with CG module has a stronger representation ability. After that, we use a task-specific head network for dealing with both oriented and horizontal object detection tasks in aerial images. ResNet [24] is used as the backbone network.

From the presentation form of bounding boxes, oriented object detection can be more suitable for aerial object detection, because it contains the orientation information of objects with more accurate bounding-box. In this work, we consider both oriented and horizontal aerial object detection tasks and develop a pipeline line to benefit both of them.

B. Feature Calibration over Images.

The purpose of feature calibration is to refine feature maps through the existing information, so as to further improve the representation ability. Currently, most of the state-of-the-art methods are designed from the perspective of feature calibration to deal with the challenges of complex background and noise in object detection [15]–[17], [19], [22]. Among those methods, attention-based ones are proposed to calibrate features from two aspects, including spatial-attention and channel-attention-based.

Spatial-attention-based mechanisms capture object positions in the spatial dimension. Position attention module [17]/Non-local operation [19] build rich contexts on local features by using a self-attention mechanism. Transformer [43] is the first sequence transduction model combined with multi-headed self-attention. DETR [18] is proposed to explore the relationship between objects in the global context, which is of precision

similar to those of the two-stage detectors, but has a weakness on detecting large objects with high computational overheads. In aerial image analysis, ARCNet [6] utilizes a recurrent attention structure to squeeze high-level semantic features for learning to reduce parameters. Channel-attention-based mechanisms allocate resources for channels referring to their importance. SENet [22] utilizes a squeeze-and-excitation block to implement dynamic channel-wise feature re-calibration. For obtaining better feature representations, DANet [17] utilizes a channel attention module to capture contextual relationships based on the self-attention mechanism. In aerial image, a residual-based network combining channel attention [14] is used to learn the most relevant high-frequency features.

There are also some works that combine spatial attention with channel-wise attention together, *e.g.*, SCA-CNN [21], and DONet [44]. These methods take advantage of both channel-wise attention and spatial-wise attention. Besides, to address considerable interference of complex background in aerial detection, multi-scale spatial and channel-wise attention mechanism [15] is proposed to strengthen the object region in aerial detection task. Despite the success of the existing attention-based methods, they are not sufficient for feature calibration in channels. In this work, we propose a simple yet effective CG scheme to enhance channel communications in a feature transformer fashion, which can adaptively determine

the calibration weights for each channel based on the global feature affinity-pairs.

III. METHODOLOGY

In this section, we show the technical details of our proposed Calibrated-Guidance Network (CG-Net) for object detection in aerial images. Specifically, we first revisit the channel attention mechanism on images in Section III-A. Then, our proposed Calibrated-Guidance (CG) module which can enhance channel communications is described in Section III-B. After that, we introduce how to implement CG on the base CNNs' feature maps (*i.e.*, Base CG) and on an intra-network feature pyramid (*i.e.*, Rearranged Pyramid CG) for object detection in aerial images in Section III-C and Section III-D. Finally, we show the details of the network architecture in Section III-E.

A. Channel Attention Revisited

Channel-wise Attention (CA) module utilizes the inter-dependencies between the channels to emphasize the important ones by weighting the similarity matrix. To be specific, CA operates on queries (\mathbf{Q}), keys (\mathbf{K}) and values (\mathbf{V}) among a set of single-scale feature maps \mathbf{X} , and the improved version \mathbf{X}' has the same scale as the original \mathbf{X} . For a given set of feature maps $\mathbf{X} \in \mathbb{R}^{W \times H \times C}$, where W , H and C are width, height and channel dimension, respectively, CA implementation can be formulated as:

$$\begin{aligned} \text{Input} &: \mathbf{q}_i, \mathbf{k}_j, \mathbf{v}_j \\ \text{Similarity} &: \mathbf{s}_{i,j} = F_{\text{sim}}(\mathbf{q}_i, \mathbf{k}_j) \\ \text{Weight} &: \mathbf{w}_{i,j} = F_{\text{nom}}(\mathbf{s}_{i,j}) \\ \text{Output} &: \mathbf{X}'_i = \sum_j F_{\text{mul}}(\mathbf{w}_{i,j}, \mathbf{v}_j), \end{aligned} \quad (1)$$

where $\mathbf{q}_i = f_q(\mathbf{X}_i) \in \mathbf{Q}$ is the i^{th} query; $\mathbf{k}_j = f_k(\mathbf{X}_j) \in \mathbf{K}$ and $\mathbf{v}_j = f_v(\mathbf{X}_j) \in \mathbf{V}$ are the j^{th} key/value pair; $f_q(\cdot)$, $f_k(\cdot)$ and $f_v(\cdot)$ denote the query/key/value channel transformer functions [18], [43]; \mathbf{X}_i and \mathbf{X}_j denote the i^{th} and j^{th} channel feature in \mathbf{X} ; F_{sim} is the dot product similarity function; F_{nom} is the softmax normalization function; F_{mul} denotes matrix dot multiplication; \mathbf{X}'_i is the i^{th} channel feature in the transformed feature map \mathbf{X}' , and the response of i^{th} channel feature is computed by j^{th} ones that enumerates all possible channels. Although CA can enable different channels to obtain different weights, the coarse operation based on the entire channel feature maps (*i.e.*, without the grouped feature representations [25], [29], [30], [43]) cannot enable all the channels to have sufficient communications, which has been empirically shown its importance in a large range of computer vision tasks. As a result, the ability to feature representation is limited.

B. Calibrated-Guidance (CG)

We propose CG to enhance feature channel communications in a feature transformer fashion, which can adaptively determine the calibration weights for the channels based on the global feature affinity-pairs. Its detailed structure is illustrated in Figure 2. CG is inspired by the transformer

mechanism and the difference is that we combine the multi-head representations, and concatenate the original feature maps and the calibrated features, then use a convolution layer to produce the enhanced feature maps as output.

Multi-head CG. We deploy the multi-head architecture to focus on richer channel feature representations. Multi-head in ViT [45] and DETR [18] can provide more feature selection when extracting features. Multi-head structure complements features by learning different contents, which is more sufficient than one head. Analysis work [46] finds that important ones in multi-head have one or more specialized and interpretable functions in the model, which indirectly shows the necessity of adopting multi-head structure.

First, we divide query and key into N parts in the channel dimension. Then, we feed the divided feature with shape $(B, C/N, H, W)$ into each head, where each structure is a CG module (B is batch size). For n^{th} head module, the shape of similarity matrix \mathbf{s}^n is $(B, C/N, C/N)$, which can be expressed as:

$$\mathbf{s}^n = \begin{bmatrix} w^{nC/N, nC/N} & \dots & w^{(n+1)C/N, 0} \\ \vdots & \ddots & \vdots \\ w^{0, (n+1)C/N} & \dots & w^{(n+1)C/N, (n+1)C/N} \end{bmatrix}, \quad (2)$$

where each w denotes the learnable similarity scalar. After that, the outputs of these head modules (*i.e.*, the partial result) are concatenated together to produce the holistic output feature maps, which have the same shape as the original feature maps. The above process can be formulated as:

$$\begin{aligned} \text{Weight} &: \mathbf{w}_{i,j}^n = F_{\text{nom}}(\mathbf{s}_{i,j}^n) \\ \text{Partial Result} &: \mathbf{X}'_i = \sum_j F_{\text{mul}}(\mathbf{w}_{i,j}^n, \mathbf{v}_{j,n}) \\ \text{Holistic Output} &: \mathbf{X}' = F_{\text{con}}(\mathbf{X}'_i), \end{aligned} \quad (3)$$

where $\mathbf{s}_{i,j}^n$ and $\mathbf{w}_{i,j}^n$ denote the n^{th} partial similarity weight of the i^{th} and j^{th} channel features and the normalized one. The i^{th} channel feature is calculated by other channel features. $\mathbf{v}_{j,n}$ denotes the j^{th} value of the n^{th} head. F_{con} is used for feature concatenation in the channel dimension. Compared to the previous transformer-based approaches, the multi-head CG has lower computational complexity, $O(NC^2)$ both in time and space, while the previous ones have the computational complexity of $O(NH^2W^2)$. Compared to CA, our proposed CG implements on pyramid features have the following three advantages: (i) CG is designed for the enhancement of communications within and between feature pyramid layers, while most of the previous ones are used to capture the long-range dependencies in space and channel within features. (ii) CG is based on the multi-head structure, which has its unique tendency of feature representation in different feature spaces [43], [47]. Hence CG can provide an enhanced feature representation. (iii) CG is designed for object detection in aerial images. By enhancing feature pyramid representation, CG can solve complex background and worse imaging quality problems in aerial images, then obtain a more accurate proposals in head network (in Section IV-B). Experimental results (Section IV-C) show that CG can improve the state-of-the-art performance swimmingly on both oriented

and horizontal tasks. Two CG implements of Base CG and Rearranged Pyramid CG show as follows.

C. Base CG

Given an arbitrary aerial image, we can extract a set of feature maps by a fully convolution network. For these feature maps, CG can directly achieve calibrated-guidance practice to enhance channel communications and adaptively determine the calibration weight for each channel. Its detailed architecture in a level of the feature pyramid (*i.e.*, feature maps with the same scale) is illustrated in Figure 2 (b). Since this CG implementation is performed on the basic feature maps, we call it Base CG. Base CG is a general unit, which works on the backbone network.

Compared to other existing head-network-based task-specific methods [4], [48], it is more universal and can facilitate a wide range of downstream recognition tasks. Our Base CG improves feature extraction, and the results can be seen from the ablation experiments shown in Section IV-B.

D. Rearranged Pyramid CG

Feature pyramid has shown its effectiveness in a wide range of computer vision tasks [8], [23], [49]. In this section, we show how to implement our Calibrated-Guidance on a feature pyramid (*i.e.*, the proposed Rearranged Pyramid CG (RP-CG)). Compared to the existing feature calibration methods on the in-network feature pyramid [50]–[52], our RP-CG has lower computational complexity and fewer model parameters (details are shown in Section IV-A). The RP-CG module works on an extracted feature pyramid from the feature pyramid network [23], whose architecture is illustrated in Figure 2 (c).

From the perspective of levels inside the feature pyramid, each level can be seen as local features, *i.e.*, only part of the features of the input image are captured. In order to emphasize the most suitable feature in the channel dimension of the feature pyramid, combining global and local information is crucial in feature extraction. In our work, RP-CG focuses on weighting different features among pyramid levels \mathbf{X}_{P2-P6} . As illustrated in Figure 2 (c), we apply CG between the levels of the feature pyramid to communicate levels' information. In our implementation, firstly, we reduce the channel dimension and launch interpolation on pyramid features \mathbf{X}_{P2-P6} to generate the same scale features (same scale as the largest one: $P2$) and then concatenate them as $\bar{\mathbf{X}}_{P2-P6}$, which is expressed as:

$$\bar{\mathbf{X}}_{P2-P6} = F_{\text{intp}}(\mathbf{X}_{P2-P6}), \quad (4)$$

where F_{intp} is a channel dimension reduction and scale interpolation function. The shape of output feature $\bar{\mathbf{X}}_{P2-P6}$ is $(B, 5, H_{p2}, W_{p2})$. Then, same as Base CG, RP-CG produces the output $\bar{\mathbf{X}}'_i$ from input $\mathbf{q}_i, \mathbf{k}_j$ and \mathbf{v}_j by learning the weight

between the query and the key. The interaction is formulated as:

$$\begin{aligned} \text{Input} &: \mathbf{X}_{P2-P6} \\ \text{Interpolation} &: \bar{\mathbf{X}}_{P2-P6} \\ \text{Extraction} &: \mathbf{q}_i, \mathbf{k}_j, \mathbf{v}_j \\ \text{Similarity} &: \mathbf{s}_{i,j} = F_{\text{sim}}(\mathbf{q}_i, \mathbf{k}_j) \\ \text{Weight} &: \mathbf{w}_{i,j} = F_{\text{nom}}(\mathbf{s}_{i,j}) \\ \text{Output} &: \bar{\mathbf{X}}'_i = \sum_j F_{\text{mul}}(\mathbf{w}_{i,j}, \mathbf{v}_j) \\ \text{Holistic Output} &: \bar{\mathbf{X}}_{P2-P6}^{\text{rpcg}} = F_{\text{con}}(\bar{\mathbf{X}}'_i), \end{aligned} \quad (5)$$

where $\bar{\mathbf{X}}'_i$ is the i^{th} level feature in transformed feature map $\bar{\mathbf{X}}_{P2-P6}^{\text{rpcg}}$ with shape $(B, 5, H_{p2}, W_{p2})$. $\bar{\mathbf{X}}_{P2-P6}^{\text{rpcg}}$ realizes global channel communication in pyramid features, but we need to find the right way to feed back to pyramid features.

In addition, there have been multitudes of methods to verify the effectiveness of the combination of global and local information in visual recognition, and our method is global in essence. To this end, combining our RP-CG with the existing local channel attention method is a natural choice. In this work, the classical channel attention [22] is chosen. Based on this, the overall structure of our proposed Rearrange Pyramid Calibrated-Guidance module can be expressed as:

$$\begin{aligned} \text{Weight} &: \bar{\mathbf{X}}_{P2-P6}^{\text{mean(rpcg)}} = F_{\text{mean}}(\bar{\mathbf{X}}_{P2-P6}^{\text{rpcg}}) \\ \text{Scale} &: \bar{\mathbf{X}}'_{P2-P6} = \bar{\mathbf{X}}_{P2-P6}^{\text{mean(rpcg)}} \otimes \mathbf{X}_{P2-P6} \\ \text{Output} &: \bar{\mathbf{X}}_{P2-P6}^{\text{final}} = F_{\text{conv}}(\bar{\mathbf{X}}'_{P2-P6} \oplus \mathbf{X}_{P2-P6}). \end{aligned} \quad (6)$$

The output from $\bar{\mathbf{X}}_{P2-P6}$ are divided into 5 parts ($P2-P6$). $\bar{\mathbf{X}}_{P2-P6}^{\text{rpcg}}$ is the overall feature after we have weighted $\bar{\mathbf{X}}_{P2-P6}$. We use F_{mean} to derive the weighting parameter to distinguish different scales' features, and it includes the operation of using the mean value as the weighting parameter for each pyramid's levels, which is then resized to the same scale of the original level feature. \otimes is matrix cross multiplication, and \oplus is channel concatenation. $\bar{\mathbf{X}}'_{P2-P6}$ is the calibrated feature with the same size as the original feature pyramid. We get final output $\bar{\mathbf{X}}_{P2-P6}^{\text{final}}$ from convolution F_{conv} , which is to reduce the channel to the original size.

E. Network Architecture

CG can help the model learn richer communication information between feature channels, so it is suitable for object detection task in aerial images. In this paper, we build a Calibrated-Guidance network (CG-Net) for both oriented and horizontal object detection tasks of aerial images. The overall architecture is illustrated in Figure 2. CG-Net is based on our proposed **Base CG** (in Figure 2 (b)) and **RP-CG** (in Figure 2 (c)) for transforming pyramid features. Specifically, we deploy ResNet [24] as backbone following [1], which has been pre-trained on the ImageNet [53]. Then, we produce a feature pyramid from the feature pyramid network [23]. For this feature pyramid, we firstly apply **Base CG** in the feature maps from each level of the pyramid. After that, we deploy the **RP-CG** to produce a new feature pyramid that realizes global and local communication in the feature

pyramid. Then, we concatenate the original feature maps with the calibrated ones together in the channel dimension and reduce the dimensionality of the concatenated feature maps into 256 channels by a 3×3 convolution. Finally, we use the head network from the RoI transformer [1] for oriented object detection and a standard Faster R-CNN [11] for horizontal object detection.

IV. EXPERIMENTS

To demonstrate the effectiveness and efficiency of our proposed method, experiments are carried out on both oriented object detection task and horizontal object detection task in aerial images. In what follows, we first show experiments settings including datasets, image size, baseline model, hyper-parameters, implementation details and evaluation metrics in Section IV-A. Then we show some ablation results including some quantitative and qualitative experimental results in Section IV-B. Finally, we show result comparisons with state-of-the-art methods in Section IV-C.

A. Settings

Datasets. In our work, two challenging datasets are selected in experiments, which are A Large-Scale Dataset for Object Detection in Aerial Images (DOTA) dataset [12] and High Resolution Ship Collections 2016 (HRSC2016) dataset [31]. DOTA is used for both oriented and horizontal object detection. HRSC2016 is used for only oriented object detection.

- **DOTA** [12] is one of the largest datasets for object detection in aerial images with both oriented and horizontal bounding box annotations. It contains 2,806 aerial images with 188,282 annotated instances from different sensors and platforms. The image size ranges from around 800×800 to $4,000 \times 4,000$ pixels and contains objects exhibiting in a wide variety of scales, orientations, and shapes. DOTA contains 15 common object categories, including Plane (PL), Baseball diamond (BD), Bridge (BR), Ground track field (GTF), Small vehicle (SV), Large vehicle (LV), Ship (SH), Tennis court (TC), Basketball court (BC), Storage tank (ST), Soccer-ball field (SBF), Roundabout (RA), Harbor (HA), Swimming pool (SP), and Helicopter (HC). In our experiments, following [4], [12], 3/6 of the original images are randomly selected as the training set, 1/6 as the validation set, and 2/6 as the testing set.
- **HRSC2016** [31] is a challenging dataset for ship detection in aerial images with large aspect ratios and arbitrary orientations, which contains 1061 images and more than 20 categories of ships in various appearances. These images are collected from Google Earth. The image size ranges from 300×300 to 1500×900 . In our work, following [31], the training, validation, and test sets include 436 images, 181 images, and 444 images, respectively. It's worth noting that only oriented object detection can be carried out for this dataset.

Image size. Due to inconsistent image sizes in the experimental datasets and taking into account the training efficiency

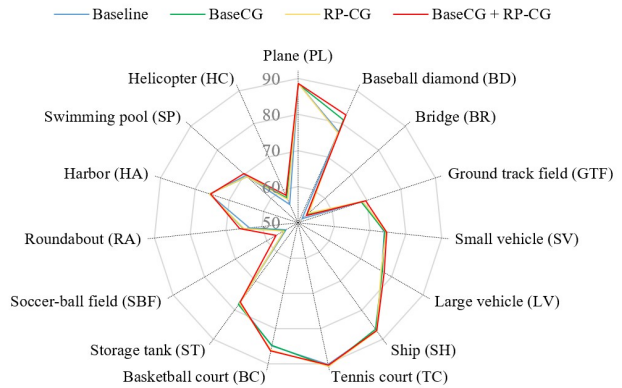


Fig. 3: Radar chart for each category of object in DOTA [12] dataset. Different colored lines represent different detectors. The larger areas enclosed by the outer line, the better recognition performance of the corresponding method. The value in this figure denotes the mAP.

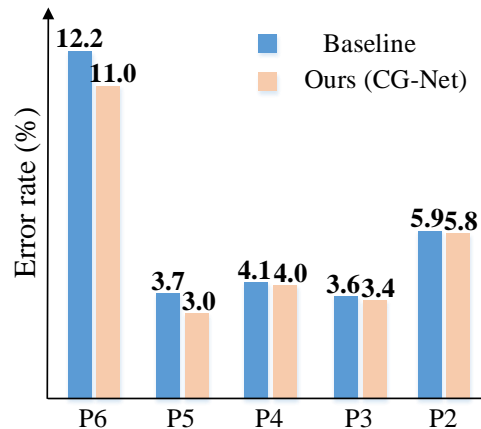


Fig. 4: Mismatching error rate comparison between the baseline and the proposed method on DOTA [12] with ResNet-101 [24] for oriented object detection. The lower the better.

and effect, for DOTA and HRSC2016, we generate a series of $1,024 \times 1,024$ patches from the original images with a stride of 824 for training, validation, and test sets, respectively.

Baseline. We use the standard two-stage detector Faster R-CNN [11] as the baseline model. It utilizes ResNet-101 as the backbone. FPN [23] is adopted to construct a feature pyramid. Predefined horizontal anchors are set on each feature level, *i.e.*, P2 - P6. The whole network is trained by an end-to-end manner. It's worth noting that we do not use any rotation anchor. For oriented object detection, we add the rotated head developed in RoI-Transformer [1] which transforms the horizontal proposals to the rotated ones. For a fair comparison, all the experimental data and parameter settings are strictly consistent as those reported in [1], [12], [31].

Hyper-parameters. Although experience shows that the adjustment of hyperparameters is conducive to the further improvement of model performance, it is necessary for the fairness of comparison. In this paper, following [1], [2], in

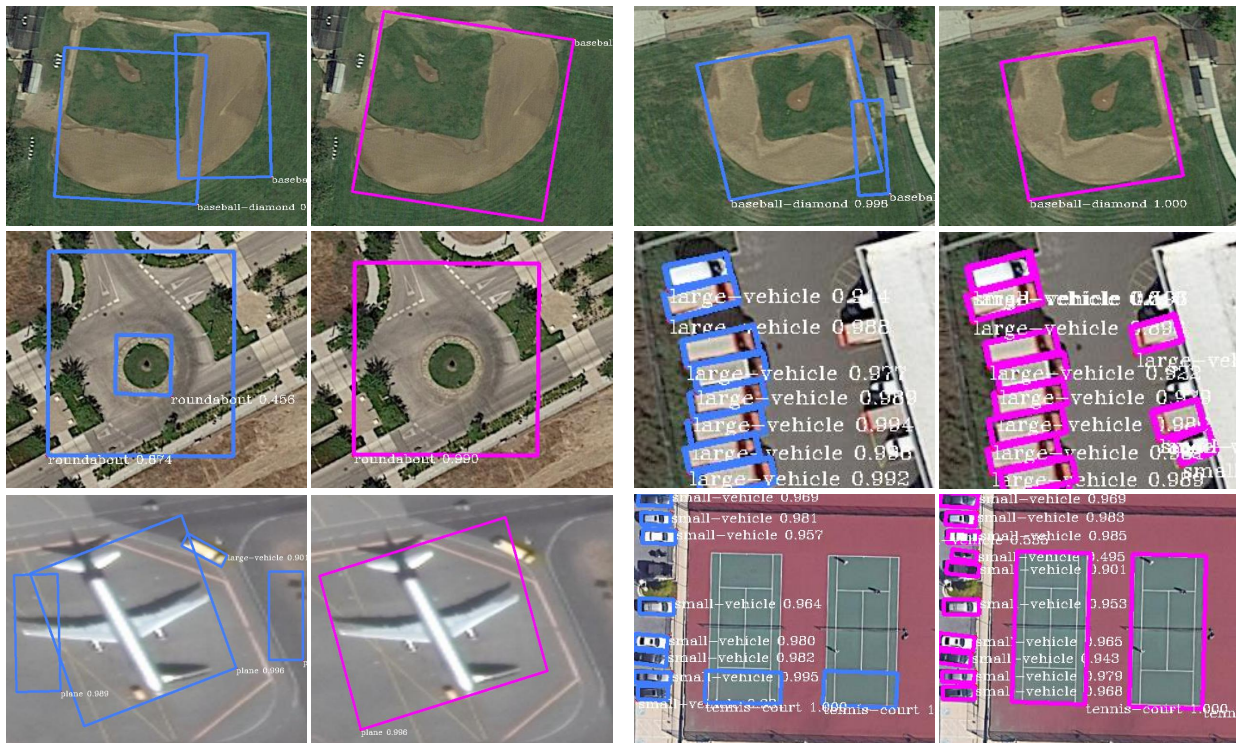


Fig. 5: Comparison to the baseline on DOTA [12] for oriented object detection with ResNet-101 [24]. The figures with blue boxes are the results of the baseline and pink boxes are the results of our proposed CG-Net.

Backbone	+Ours	GFLOPs / FPS	#Params (M)	mAP (%)
ResNet-50	✗	211.30 / 25.0	41.20	73.26
	✓	366.32 / 14.8	42.99	74.21+0.95
ResNet-101	✗	289.26 / 20.9	60.19	73.06
	✓	444.21 / 13.4	61.98	74.30+1.24
ResNet-152	✗	367.23 / 17.0	75.83	72.78
	✓	522.19 / 12.1	77.63	73.53+0.75

TABLE I: The effectiveness of our proposed methods with different backbone networks on the test set of DOTA [12] for oriented object detection. “+ Ours” indicates the implementation of our proposed Base CG and RP-CG units on the backbone networks.

DOTA and HRSC2016, only three horizontal anchors are set with aspect ratios of $\{1/2, 1, 2\}$, the base anchor scale is set as $\{8^2\}$, and the anchor strides of each level of the feature pyramid are set as $\{4, 8, 16, 32, 64\}$. In order to verify the effectiveness of our method, we performed ablation studies on DOTA dataset, and we avoid utilizing any bells-and-whistles training strategy and data augmentation in the ablation study. But for the peer comparison on DOTA and HRSC2016, like [1], [2], [4], we only conduct a rotation augmentation randomly from 4 angles (0, 90, 180, 270).

Implementation details. In our work, SGD is used as the optimizer in the training stage. The initial learning rate is set to 0.005 and is divided by 10 at each decay step. Weight decay and momentum are set to 0.0001 and 0.9, respectively. Follow-

ing [12], [31], the total iterations of DOTA and HRSC2016 are 80k and 20k, respectively. We train the models on RTX 2080Ti with a batch size of 1. Besides, during the model testing phase, we did not use any testing strategies, *e.g.*, data augmentation or multi-scale testing.

Evaluation metrics. Following [12], the standard mean Average Precision (mAP) is used as the primary evaluation metric in accuracy. Moreover, to verify the model efficiency, the model Parameters (#Params), and GFLOPs / FPS are also taken into consideration. The results of DOTA reported in our work are obtained by submitting our predictions to the official DOTA evaluation server¹.

B. Ablation Study

Our ablation study is carried out on DOTA [12] for oriented object detection with ResNet-101 [24] as the backbone network, which aims to: (1) verify the effectiveness of our method on different backbone networks; (2) verify the effectiveness of the two proposed units on base CNN feature maps (*i.e.*, Base CG) and a feature pyramid (*i.e.*, RP-CG); (3) reveal mismatching error rates on different scales; and (4) show some visual comparisons. The details are as follows:

(1) **Effectiveness on different backbones.** In Table I, we show the experimental results of different backbone networks with our proposed units on the test set of DOTA. We contrast mAP and its improvement from the combination of our proposed module with ResNet-50, ResNet-101, and ResNet-152, respectively. We can observe that adding our proposed module

¹<https://captain-whu.github.io/DOTA/>

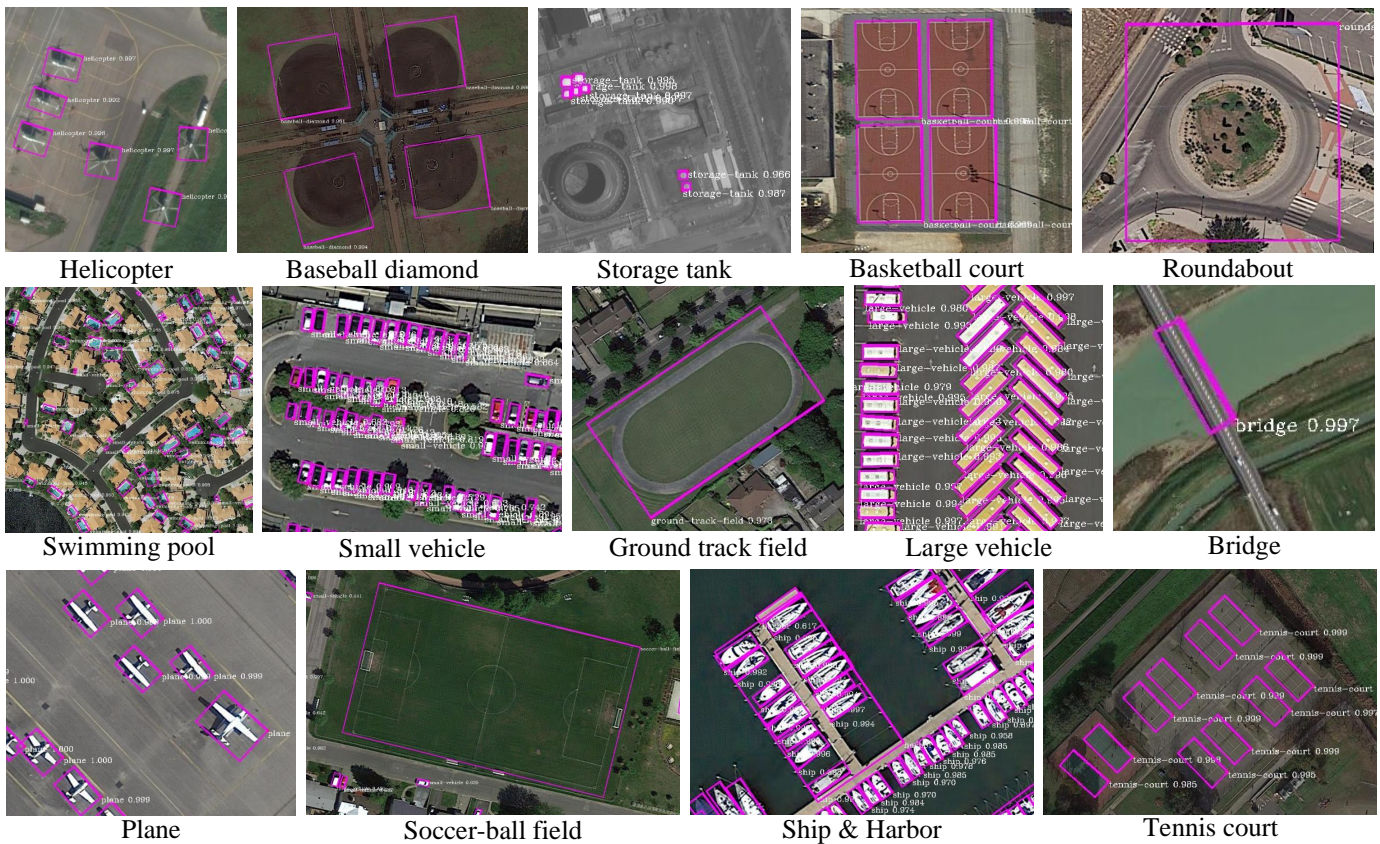


Fig. 6: Visualization results for oriented object detection on the test set of DOTA [12]

to the backbone increases mAP by 0.95%, 1.24%, and 0.75%. Besides, we also report the model #Params and GFLOPs / FPS for comparisons of model efficiency. Using Base CG and RP-CG increases computational costs; for example, average increases on these three backbones are around 1.80 M model #Params with around 155 GFLOPs, and with around 5-10 FPS reduction. Considering the model performance and the amount of calculation, in the following experiments, we select ResNet-101 as our backbone network.

(2) Effectiveness of the proposed units. In Table II, we show the units and their combined performance on ResNet-101. We can observe that Base CG and RP-CG respectively bring 0.58% and 0.46% improvements for the bounding box mAP. The corresponding each-category mAP radar chart for oriented object detection is in Figure 3, to show the trend of the performance change. Combining Base CG and RP-CG together (*i.e.*, our proposed CG-Net), the model can increase mAP by at most 1.24%, in which some categories have large improvements, such as BD (Baseball diamond) 5.05%, SBF (Soccer-ball field) 3.14%, and RA (Roundabout) 2.77%. These results indicate that the feature presentation capabilities have been further improved by Base CG and RP-CG. As for the model efficiency, we can observe that Base CG and RP-CG respectively brings 0.59 and 0.61 M model #Params with 51.53 and 51.89 GFLOPs. When these two models are deployed together, there are 1.79 M model #Params and 154.95 GFLOPs increment. Our proposed CG is based on self-attention and calculates the similarity matrix between features,

so that GFlops increases from 289.26 to 444.21. The increase in computational complexity is also a common problem for models based on the self-attention mechanism.

(3) Improving RPN input for aerial object detection. CG-Net shows significance when addressing complex background and worse imaging quality problems. Aerial images have complex geological structures, objects with different size and object categories due to overhead shots from high altitude, so they have a more complex background. In aerial object detection, worse imaging quality is detrimental to learn object features and directly affects model training. Therefore, we implement CG on pyramid features with Base CG and Rearrange Pyramid CG. In pyramid features, the size of proposals from Region Proposal Network (RPN) [11] depends on the maximum response layer. Therefore, whether object proposals selected accurately will affect the difficulty of ROI module in training the detection box, which requires more accurate pyramid features. CG-Net can help model learn richer communication information within and between each layer of pyramid features. To sum up, making Calibrated-Guidance operation for pyramid features is essential before input into region proposal network.

(4) Mismatching error rates on different scales. To reveal the effect of the proposed method on each level of the feature map, we define mismatching error rates on different scales in the feature pyramid, *i.e.*, the selected level of each object is not consistent with the ground-truth level. It can be seen from Figure 4 that the mismatching error rate of each layer in the

Baseline	Base CG	RP-CG	PL	BD	BR	GTF	SV	LV	SH	TC	BC	ST	SBF	RA	HA	SP	HC	GFLOPs / FPS	#Params	mAP (%)
✓	✗	✗	88.53	77.70	51.59	68.80	74.02	76.85	86.98	90.24	84.89	77.68	53.91	63.56	75.88	69.48	55.50	289.26 / 20.9	60.19 M	73.06
✓	✓	✗	88.38	81.09	53.43	68.35	74.23	76.95	86.55	90.67	84.79	78.17	54.20	65.23	75.84	69.01	57.64	340.79 / 19.0	60.78 M	73.64 ^{+0.58}
✓	✗	✓	88.49	77.18	54.02	68.85	74.49	76.67	87.09	90.79	86.17	77.58	54.54	65.03	75.87	69.11	56.94	341.15 / 17.2	60.80 M	73.52 ^{+0.46}
✓	✓	✓	88.65	82.75	53.02	69.65	74.77	77.48	86.99	90.32	86.38	77.23	57.05	66.33	75.46	70.22	58.23	444.21 / 13.4	61.98 M	74.30 ^{+1.24}

TABLE II: Ablation study on the test set of DOTA [12] for oriented object detection. ResNet-101 [24] is the backbone.

Methods	Backbone	PL	BD	BR	GTF	SV	LV	SH	TC	BC	ST	SBF	RA	HA	SP	HC	mAP (%)
Oriented object detection																	
FR-O [12] (CVPR 2018)	R-101	79.09	69.12	17.17	63.49	34.20	37.16	36.20	89.19	69.60	58.96	49.40	52.52	46.69	44.80	46.30	52.93
R-DFPN [54] (RS 2018)	R-101	80.92	65.82	33.77	58.94	55.77	50.94	54.78	90.33	66.34	68.66	48.73	51.76	55.10	51.32	35.88	57.94
R ² CNN [39] (preprint 2017)	R-101	80.94	65.67	35.34	67.44	59.92	50.91	55.81	90.67	66.92	72.39	55.06	52.23	55.14	53.35	48.22	60.67
RRPN [55] (TMM 2018)	R-101	88.52	71.20	31.66	59.30	51.85	56.19	57.25	90.81	72.84	67.38	56.69	52.84	53.08	51.94	53.58	61.01
ICN [56] (ACCV 2018)	R-101	81.36	74.30	47.70	70.32	64.89	67.82	69.98	90.76	79.06	78.02	53.64	62.90	67.02	64.17	50.23	68.16
RoI Trans [1] (CVPR 2019)	R-101	88.64	78.52	43.44	75.92	68.81	73.68	83.59	90.74	77.27	81.46	58.39	53.54	62.83	58.93	47.67	69.56
CAD-Net [57] (TGRS 2019)	R-101	87.80	82.40	49.40	73.50	71.10	63.50	76.70	90.90	79.20	73.30	48.40	60.90	62.00	67.00	62.20	69.90
DRN [58] (CVPR 2020)	H-104	88.91	80.22	43.52	63.35	73.48	70.69	84.94	90.14	83.85	84.11	50.12	58.41	67.62	68.60	52.50	70.70
O ² -DNet [41] (ISPRS 2020)	H-104	89.31	82.14	47.33	61.21	71.32	74.03	78.62	90.76	82.23	81.36	60.93	60.17	58.21	66.98	61.03	71.04
SCRDet [4] (ICCV 2019)	R-101	89.98	80.65	52.09	68.36	68.36	60.32	72.41	90.85	87.94	86.86	65.02	66.68	66.25	68.24	65.21	72.61
CFC-Net [38] (TGRS 2021)	R-50	89.08	80.41	52.41	70.02	76.28	78.11	87.21	90.89	84.47	85.64	60.51	61.52	67.82	68.02	50.09	73.50
R ³ Det [40] (AAAI 2021)	R-152	89.49	81.17	50.53	66.10	70.92	78.66	78.21	90.81	85.26	84.23	61.81	63.77	68.16	69.83	67.17	73.74
CSL [3] (ECCV 2020)	R-152	90.25	85.53	54.64	75.31	70.44	73.51	77.62	90.84	86.15	86.69	69.60	68.04	73.83	71.10	68.93	76.17
DAL [2] (AAAI 2021)	R-50	89.69	83.11	55.03	71.00	78.30	81.90	88.46	90.89	84.97	87.46	64.41	65.65	76.86	72.09	64.35	76.95
R ³ Det-DCL [5] (CVPR 2021)	R-152	89.26	83.60	53.54	72.76	79.04	82.56	87.31	90.67	86.59	86.98	67.49	66.88	73.29	70.56	69.99	77.37
Ours (CG-Net)	R-101	88.75	85.18	57.41	71.88	73.23	82.68	88.14	90.90	86.00	85.37	62.99	66.74	77.98	79.90	71.27	77.89 ^{+0.52}
Horizontal object detection																	
SSD [59] (ECCV 2016)	R-101	44.74	11.21	6.22	6.91	2.00	10.24	11.34	15.59	12.56	17.94	14.73	4.55	4.55	0.53	1.01	10.94
YOLOv2 [9] (CVPR 2016)	R-101	76.90	33.87	22.73	34.88	38.73	32.02	52.37	61.65	48.54	33.91	29.27	36.83	36.44	38.26	11.61	39.20
YOLOv5 [60] (Github 2020)	D-53	70.01	43.26	19.36	36.02	29.77	29.51	53.24	71.34	55.75	34.68	36.70	43.21	42.42	41.8	21.4	43.31
R-FCN [33] (NIPS 2016)	R-101	79.33	44.26	36.58	53.53	39.38	34.15	47.29	45.66	47.74	65.84	37.92	44.23	47.23	50.64	34.90	47.24
FR-H [12] (CVPR 2018)	R-101	80.32	77.55	32.86	68.13	53.66	52.49	50.04	90.41	75.05	59.59	57.00	49.81	61.69	56.46	41.85	60.46
FPN [23] (CVPR 2017)	R-101	88.70	75.10	52.60	59.20	69.40	78.80	84.50	90.60	81.30	82.60	52.50	62.10	76.60	66.30	60.10	72.00
ICN [56] (ACCV 2018)	R-101	90.00	77.70	53.40	73.30	73.50	65.00	78.20	90.80	79.10	84.80	57.20	62.10	73.50	70.20	58.10	72.50
SCRDet [4] (ICCV 2019)	R-101	90.18	81.88	55.30	73.29	72.09	77.65	78.06	90.91	82.44	86.39	64.53	63.45	75.77	78.21	60.11	75.35
Ours (CG-Net)	R-101	88.76	85.36	60.81	71.88	74.04	83.43	88.29	90.89	86.00	85.55	63.51	67.02	78.78	80.86	68.70	78.26 ^{+2.91}

TABLE III: Result comparisons with state-of-the-art methods on the test set of DOTA [12] for both oriented and horizontal object detection in aerial images. By “Ours” we mean that implementing Base CG and RP-CG on the baseline model at the same time. “R-” in the Backbone column denotes the ResNet [24], “D-” in the Backbone column denotes the DarkNet [9], and “H-” denotes the Hourglass network [61].

feature pyramid has been reduced after deploying our proposed method (*i.e.*, the joint implementation of Base CG and RP-CG). Compared with the low-level feature in the feature pyramid that is more suitable for small objects, the reduction of error rates in high-level is obvious. For example, there are 0.1%, 0.2%, 0.1%, 0.7%, and 1.2% error rate reduction from level P_2 to P_6 . Therefore, the effectiveness of our method can be further confirmed.

(5) Visualizations. From results of Ablation Experiment Table III and Figure 6, complex background and worse imaging quality, showing like Baseball diamond (BD), Ground track field (GTF), Plane (PL) and Roundabout (RA), can be seen as obvious problems. Specifically, when detecting boxes as used to cover the whole objects, the boundary of boxes may

show certain fuzziness, such as class Roundabout in Figure 5 left line 2, the problem of which is affected by complex background and labeling for completely covering object in aerial data. In left line 3, worse imaging quality leads to additional false detection box in local areas.

C. Comparisons with state-of-the-arts

Results on DOTA. The experimental result on the test set of DOTA is shown in Table III. The each-category mAP radar chart for oriented object detection is in Figure 7 and for horizontal object detection is in Figure 8, to show the trend of the performance change. CG-Net achieves the best score by 77.89% mAP for oriented object detection and 78.26% mAP for horizontal object detection. Considering the 15 categories,

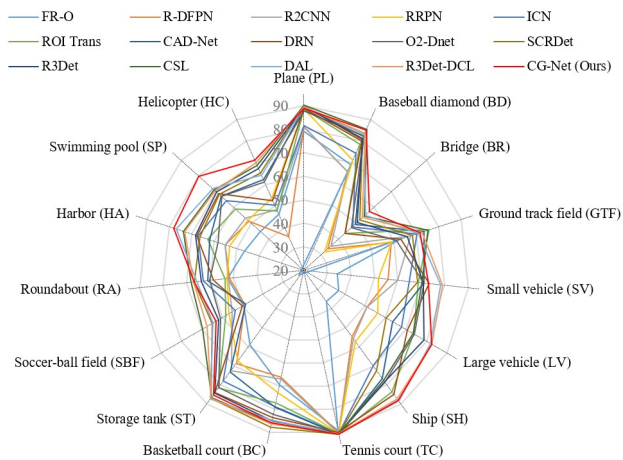


Fig. 7: Radar chart for the state-of-the-art methods on DOTA [12] dataset for oriented object detection. Different colored lines represent different detectors. The larger areas enclosed by the outer line, the better recognition performance of the corresponding method. The value in this figure denotes the mAP.

Methods	Backbone	mAP (%)
R ² CNN [39] (preprint 2017)	R-101	73.07
RCI&RC2 [31] (ICPRAM 2017)	V-16	75.70
RRPN [55] (TMM 2018)	R-101	79.08
R ² PN [62] (GRSL 2018)	V-16	79.60
RRD [63] (CVPR 2018)	V-16	84.30
RoI Trans [1] (CVPR 2019)	R-101	86.20
Gliding Vertex [36] (TPAMI 2020)	R-101	88.20
R-RetinaNet [8] (ICCV 2017)	R-101	89.18
R-RPN [42] (TGRS 2020)	V-16	89.20
R ³ Det [40] (AAAI 2021)	R-101	89.26
RetinaNet-DAL [2] (AAAI 2021)	R-101	89.77
R ³ Det-DCL [5] (CVPR 2021)	R-101	89.46
Ours (CG-Net)	R-101	90.58^{+1.12}

TABLE IV: Result comparisons with state-of-the-art methods on the test set of HRSC2016 [31] for oriented object detection in aerial images. “R-” in the Backbone column denotes the ResNet [24], and “V-” denotes the VGG network [64]. mAP is obtained on the VOC 2007 evaluation metric.

CG-Net ranks at the top for 6 for oriented object detection and 10 for horizontal object detection. Moreover, CG-Net surpasses the state-of-the-art by 0.52% mAP for oriented object detection with a weaker backbone network (ResNet-101 vs ResNet-152) and 2.91% mAP for horizontal object detection with the same backbone. Compared to the approach (*i.e.*, SCRDet [4]) with the same backbone network (*i.e.*, ResNet-101), our model has improved mAP by 5.82%, which is quite remarkable in today’s performance. Visualization results on the test set of DOTA are shown in Figure 6. We can clearly observe that our model can achieve accurate recognition results.

Results on HRSC2016. Result comparisons with the state-

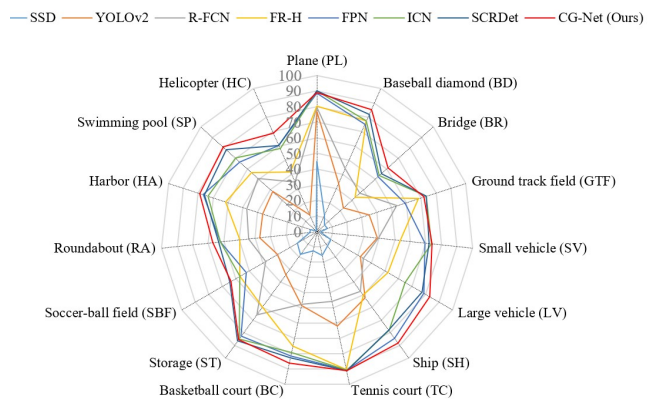


Fig. 8: Radar chart for the state-of-the-art methods on DOTA [12] dataset for horizontal object detection. Different colored lines represent different detectors. The larger areas enclosed by the outer line, the better recognition performance of the corresponding method. The value in this figure denotes the mAP.

of-the-art methods on the test set of HRSC2016 [31] are shown in Table IV. We can observe that our method achieves the state-of-the-art performance in mAP by 90.58%, which surpasses the previous best model (*i.e.*, R³Det-DCL [5]) by 1.12%. Particularly, in our experiments, our CG-Net uses only 3 horizontal anchors with aspect ratios of $\{1/2, 1, 2\}$, but outperforms the frameworks with a large number of anchors. This shows that it is critical to effectively utilize the predefined anchors to generate high-quality feature, and it may be no need to preset a large number of rotated anchors. In addition, we also believe that our model can achieve further recognition performance with more complex aspect ratios.

V. CONCLUSION

In this work, a simple yet effective CG operation was proposed to enhance channel communications in a feature transformer fashion, which can adaptively determine the calibration weights for each channel. To demonstrate its effectiveness, we implemented CG on the standard object detection backbone network with a feature pyramid network (*i.e.*, CG-Net) and conducted extensive experiments on both oriented and horizontal object detection of aerial images. Experimental results on the challenging DOTA and HRSC2016 indicated that the proposed CG-Net could achieve state-of-the-art performance in accuracy with a fair computational overhead. In the future, we will explore applying CG-Net to a broader range of natural scenes. Besides, exploring how to use CG-Net in other visual tasks (*e.g.*, semantic segmentation, person re-identification, and image generation) is also an important direction.

REFERENCES

- [1] J. Ding, N. Xue, Y. Long, G.-S. Xia, and Q. Lu, “Learning roi transformer for oriented object detection in aerial images,” in *IEEE/CVF Conference on Computer Vision and Pattern Recognition (CVPR)*, 2019.
- [2] Q. Ming, Z. Zhou, L. Miao, H. Zhang, and L. Li, “Dynamic anchor learning for arbitrary-oriented object detection,” in *Association for the Advancement of Artificial Intelligence (AAAI)*, 2021.

- [3] X. Yang and J. Yan, "Arbitrary-oriented object detection with circular smooth label," in *European Conference on Computer Vision (ECCV)*, 2020.
- [4] X. Yang, J. Yang, J. Yan, Y. Zhang, T. Zhang, Z. Guo, X. Sun, and K. Fu, "ScrDet: Towards more robust detection for small, cluttered and rotated objects," in *International Conference on Computer Vision (ICCV)*, 2019.
- [5] X. Yang, L. Hou, Y. Zhou, W. Wang, and J. Yan, "Dense label encoding for boundary discontinuity free rotation detection," in *arXiv*, 2020.
- [6] Q. Wang, S. Liu, J. Chanussot, and X. Li, "Scene classification with recurrent attention of vhr remote sensing images," in *IEEE Transactions on Geoscience and Remote Sensing*, 2018.
- [7] D. Zhang, N. Li, and Q. Ye, "Positional context aggregation network for remote sensing scene classification," *IEEE Geoscience and Remote Sensing Letters*, vol. 17, no. 6, pp. 943–947, 2019.
- [8] T.-Y. Lin, P. Goyal, R. Girshick, K. He, and P. Dollár, "Focal loss for dense object detection," in *International Conference on Computer Vision (ICCV)*, 2017.
- [9] J. Redmon, S. Divvala, R. Girshick, and A. Farhadi, "You only look once: Unified, real-time object detection," in *IEEE/CVF Conference on Computer Vision and Pattern Recognition (CVPR)*, 2016.
- [10] R. Girshick, "Fast r-cnn," in *International Conference on Computer Vision (ICCV)*, 2015.
- [11] S. Ren, K. He, R. Girshick, and J. Sun, "Faster r-cnn: Towards real-time object detection with region proposal networks," in *Neural Information Processing Systems (NeurIPS)*, 2016.
- [12] G.-S. Xia, X. Bai, J. Ding, Z. Zhu, S. Belongie, J. Luo, M. Datcu, M. Pelillo, and L. Zhang, "Dota: A large-scale dataset for object detection in aerial images," in *IEEE/CVF Conference on Computer Vision and Pattern Recognition (CVPR)*, 2018.
- [13] M. Kamiński, P. Zientara, and M. Krawczyk, "Electrical resistivity tomography and digital aerial photogrammetry in the research of the "bachledzki hill" active landslide—in podhale (poland)," in *Engineering Geology*, 2021.
- [14] J. M. Haut, R. Fernandez-Beltran, M. E. Paoletti, J. Plaza, and A. Plaza, "Remote sensing image superresolution using deep residual channel attention," in *IEEE Transactions on Geoscience and Remote Sensing*, 2019.
- [15] J. Chen, L. Wan, J. Zhu, G. Xu, and M. Deng, "Multi-scale spatial and channel-wise attention for improving object detection in remote sensing imagery," in *IEEE Geoscience and Remote Sensing Letters*, 2019.
- [16] C. Wang, X. Bai, S. Wang, J. Zhou, and P. Ren, "Multiscale visual attention networks for object detection in vhr remote sensing images," in *IEEE Geoscience and Remote Sensing Letters*, 2018.
- [17] J. Fu, J. Liu, H. Tian, Y. Li, Y. Bao, Z. Fang, and H. Lu, "Dual attention network for scene segmentation," in *IEEE/CVF Conference on Computer Vision and Pattern Recognition (CVPR)*, 2019.
- [18] N. Carion, F. Massa, G. Synnaeve, N. Usunier, A. Kirillov, and S. Zagoruyko, "End-to-end object detection with transformers," in *European Conference on Computer Vision (ECCV)*, 2020.
- [19] X. Wang, R. Girshick, A. Gupta, and K. He, "Non-local neural networks," in *IEEE/CVF Conference on Computer Vision and Pattern Recognition (CVPR)*, 2018.
- [20] Y. Yuan and J. Wang, "Ocnnet: Object context network for scene parsing," in *arXiv*, 2018.
- [21] L. Chen, H. Zhang, J. Xiao, L. Nie, J. Shao, W. Liu, and T.-S. Chua, "Sca-cnn: Spatial and channel-wise attention in convolutional networks for image captioning," in *IEEE/CVF Conference on Computer Vision and Pattern Recognition (CVPR)*, 2017.
- [22] J. Hu, L. Shen, and G. Sun, "Squeeze-and-excitation networks," in *IEEE/CVF Conference on Computer Vision and Pattern Recognition (CVPR)*, 2018.
- [23] T.-Y. Lin, P. Dollár, R. Girshick, K. He, B. Hariharan, and S. Belongie, "Feature pyramid networks for object detection," in *IEEE/CVF Conference on Computer Vision and Pattern Recognition (CVPR)*, 2017.
- [24] K. He, X. Zhang, S. Ren, and J. Sun, "Deep residual learning for image recognition," in *IEEE/CVF Conference on Computer Vision and Pattern Recognition (CVPR)*, 2016.
- [25] X. Zhang, X. Zhou, M. Lin, and J. Sun, "Shufflenet: An extremely efficient convolutional neural network for mobile devices," in *IEEE/CVF Conference on Computer Vision and Pattern Recognition (CVPR)*, 2018.
- [26] Y. Wu and K. He, "Group normalization," in *European Conference on Computer Vision (ECCV)*, 2018.
- [27] A. Howard, M. Sandler, G. Chu, L.-C. Chen, B. Chen, M. Tan, W. Wang, Y. Zhu, R. Pang, V. Vasudevan et al., "Searching for mobilenetv3," in *International Conference on Computer Vision (ICCV)*, 2019.
- [28] C. He, H. Ye, L. Shen, and T. Zhang, "Milenas: Efficient neural architecture search via mixed-level reformulation," in *IEEE/CVF Conference on Computer Vision and Pattern Recognition (CVPR)*, 2020.
- [29] I. Radosavovic, R. P. Kosaraju, R. Girshick, K. He, and P. Dollár, "Designing network design spaces," in *IEEE/CVF Conference on Computer Vision and Pattern Recognition (CVPR)*, 2020.
- [30] Z. Yang, Z. Dai, R. Salakhutdinov, and W. W. Cohen, "Breaking the softmax bottleneck: A high-rank rnn language model," in *International Conference on Learning Representations (ICLR)*, 2018.
- [31] Z. Liu, L. Yuan, L. Weng, and Y. Yang, "A high resolution optical satellite image dataset for ship recognition and some new baselines," in *International Conference on Pattern Recognition Applications and Methods (ICPRAM)*, 2017.
- [32] F. Bouhleh, H. Mliki, and M. HaACM Multimedia (MM)ami, "Abnormal crowd density estimation in aerial images based on the deep and handcrafted features fusion," in *Expert Systems with Applications*, 2021.
- [33] J. Dai, Y. Li, K. He, and J. Sun, "R-fcn: Object detection via region-based fully convolutional networks," in *Neural Information Processing Systems (NeurIPS)*, 2016.
- [34] L. Liu, Z. Pan, and B. Lei, "Learning a rotation invariant detector with rotatable bounding box," in *arXiv*, 2017.
- [35] X. Yang, K. Fu, H. Sun, J. Yang, Z. Guo, M. Yan, T. Zhan, and S. Xian, "R2cnn++: Multi-dimensional attention based rotation invariant detector with robust anchor strategy," in *arXiv*, 2018.
- [36] Y. Xu, M. Fu, Q. Wang, Y. Wang, K. Chen, G.-S. Xia, and X. Bai, "Gliding vertex on the horizontal bounding box for multi-oriented object detection," in *IEEE Transactions on Pattern Analysis and Machine Intelligence*, 2020.
- [37] W. Qian, X. Yang, S. Peng, Y. Guo, and C. Yan, "Learning modulated loss for rotated object detection," in *Association for the Advancement of Artificial Intelligence (AAAI)*, 2021.
- [38] Q. Ming, L. Miao, Z. Zhou, and Y. Dong, "Cfc-net: A critical feature capturing network for arbitrary-oriented object detection in remote sensing images," in *IEEE Transactions on Geoscience and Remote Sensing*, 2021.
- [39] Y. Jiang, X. Zhu, X. Wang, S. Yang, W. Li, H. Wang, P. Fu, and Z. Luo, "R2cnn: rotational region cnn for orientation robust scene text detection," in *arXiv*, 2017.
- [40] X. Yang, Q. Liu, J. Yan, A. Li, Z. Zhang, and G. Yu, "R3det: Refined single-stage detector with feature refinement for rotating object," in *AAAI*, 2021.
- [41] H. Wei, Y. Zhang, Z. Chang, H. Li, H. Wang, and X. Sun, "Oriented objects as pairs of middle lines," in *International Society for Photogrammetry and Remote Sensing*, 2020.
- [42] L. Li, Z. Zhou, B. Wang, L. Miao, and H. Zong, "A novel cnn-based method for accurate ship detection in hr optical remote sensing images via rotated bounding box," in *IEEE Transactions on Geoscience and Remote Sensing*, 2020.
- [43] A. Vaswani, N. Shazeer, N. Parmar, J. Uszkoreit, L. Jones, A. N. Gomez, L. Kaiser, and I. Polosukhin, "Attention is all you need," in *Neural Information Processing Systems (NeurIPS)*, 2017.
- [44] W. Zhang, D. Zhang, and X. Xiang, "Cascaded and dual: Discrimination oriented network for brain tumor classification," in *Asian Conference on Machine Learning (ACML)*, 2019.
- [45] A. Dosovitskiy, L. Beyer, A. Kolesnikov, D. Weissenborn, X. Zhai, T. Unterthiner, M. Dehghani, M. Minderer, G. Heigold, and S. Gelly, "An image is worth 16x16 words: Transformers for image recognition at scale," in *International Conference on Learning Representations (ICLR)*, 2021.
- [46] E. Voita, D. Talbot, F. Moiseev, R. Senrich, and I. Titov, "Analyzing multi-head self-attention: Specialized heads do the heavy lifting, the rest can be pruned," 2019.
- [47] I. Bello, B. Zoph, A. Vaswani, J. Shlens, and Q. V. Le, "Attention augmented convolutional networks," in *International Conference on Computer Vision (ICCV)*, 2019.
- [48] Y. Lin, P. Feng, and J. Guan, "Ienet: Interacting embranchment one stage anchor free detector for orientation aerial object detection," in *arXiv*, 2019.
- [49] D. Zhang, H. Zhang, J. Tang, M. Wang, X. Hua, and Q. Sun, "Feature pyramid transformer," in *European Conference on Computer Vision (ECCV)*, 2020.
- [50] J. Pang, K. Chen, J. Shi, H. Feng, W. Ouyang, and D. Lin, "Libra r-cnn: Towards balanced learning for object detection," in *IEEE/CVF Conference on Computer Vision and Pattern Recognition (CVPR)*, 2019.
- [51] G. Ghiasi, T.-Y. Lin, and Q. V. Le, "Nas-fpn: Learning scalable feature pyramid architecture for object detection," in *IEEE/CVF Conference on Computer Vision and Pattern Recognition (CVPR)*, 2019.

- [52] Z. Qin, Z. Li, Z. Zhang, Y. Bao, G. Yu, Y. Peng, and J. Sun, "Thundernet: Towards real-time generic object detection on mobile devices," in *IEEE/CVF Conference on Computer Vision and Pattern Recognition (CVPR)*, 2019.
- [53] J. Deng, W. Dong, R. Socher, L.-J. Li, K. Li, and L. Fei-Fei, "Imagenet: A large-scale hierarchical image database," in *IEEE/CVF Conference on Computer Vision and Pattern Recognition (CVPR)*, 2009.
- [54] X. Yang, H. Sun, K. Fu, J. Yang, X. Sun, M. Yan, and Z. Guo, "Automatic ship detection in remote sensing images from google earth of complex scenes based on multiscale rotation dense feature pyramid networks," in *Remote Sensing*, 2018.
- [55] J. Ma, W. Shao, H. Ye, L. Wang, H. Wang, Y. Zheng, and X. Xue, "Arbitrary-oriented scene text detection via rotation proposals," in *IEEE Transactions on Multimedia*, 2018.
- [56] S. M. Azimi, E. Vig, R. Bahmanyar, M. Körner, and P. Reinartz, "Towards multi-class object detection in unconstrained remote sensing imagery," in *Asian Conference on Computer Vision (ACCV)*, 2018.
- [57] G. Zhang, S. Lu, and W. Zhang, "Cad-net: A context-aware detection network for objects in remote sensing imagery," in *IEEE Transactions on Geoscience and Remote Sensing*, 2019.
- [58] X. Pan, Y. Ren, K. Sheng, W. Dong, H. Yuan, X. Guo, C. Ma, and C. Xu, "Dynamic refinement network for oriented and densely packed object detection," in *IEEE/CVF Conference on Computer Vision and Pattern Recognition (CVPR)*, 2020.
- [59] W. Liu, D. Anguelov, D. Erhan, C. Szegedy, S. Reed, C.-Y. Fu, and A. C. Berg, "Ssd: Single shot multibox detector," in *European Conference on Computer Vision (ECCV)*, 2016.
- [60] G. Jocher, "Yolov5," 2020. [Online]. Available: <https://github.com/ultralytics/yolov5>
- [61] A. Newell, K. Yang, and J. Deng, "Stacked hourglass networks for human pose estimation," in *European Conference on Computer Vision (ECCV)*, 2016.
- [62] Z. Zhang, W. Guo, S. Zhu, and W. Yu, "Toward arbitrary-oriented ship detection with rotated region proposal and discrimination networks," in *IEEE Geoscience and Remote Sensing Letters*, 2018.
- [63] M. Liao, Z. Zhu, B. Shi, G.-s. Xia, and X. Bai, "Rotation-sensitive regression for oriented scene text detection," in *IEEE/CVF Conference on Computer Vision and Pattern Recognition (CVPR)*, 2018.
- [64] K. Simonyan and A. Zisserman, "Very deep convolutional networks for large-scale image recognition," in *International Conference on Learning Representations (ICLR)*, 2015.



Zongqi Wei received the BS degree in Computer Science and Technology at Nanjing Post and Telecommunication University, China. He is now a master student with the College of Computer Science and Technology, Nanjing University of Aeronautics and Astronautics. His research interests include computer vision, especially in object detection and video object segmentation. He is currently a research intern with TikTok.



Dong Liang received the B.S. degree in Telecommunication Engineering and the M.S. degree in Circuits and Systems from Lanzhou University, China, in 2008 and 2011, respectively. In 2015, he received Ph.D. at Graduate School of IST, Hokkaido University, Japan. He is currently an associate professor with the College of Computer Science and Technology, Nanjing University of Aeronautics and Astronautics. His research interests include model communication in pattern recognition and image processing. He was awarded the Excellence Research Award from Hokkaido University in 2013. He has published several research papers including in Pattern Recognition, IEEE TIP/TCSVT, and AAAI.



Dong Zhang received the BS degree and the MS degree in Computer Science and Technology at Nanjing Forestry University, China. He is now a Ph.D. student in School of Computer Science and Engineering, Nanjing University of Science and Technology, China. His research interests include machine learning and computer vision, especially in object detection, semantic segmentation, scene parsing, video object segmentation and cross-scene segmentation. In these areas, he has published several journal and conference papers including IEEE Transactions on Cybernetics, AAAI, IJCAI, ECCV, ICCV, and NeurIPS.



Liyan Zhang received the Ph.D. degree in computer science from the University of California, Irvine, Irvine, CA, USA, in 2014. She is currently a Professor with the College of Computer Science and Technology, Nanjing University of Aeronautics and Astronautics, Nanjing, China. Her research interests include multimedia analysis, computer vision, and deep learning. Dr. Zhang received the Best Paper Award from the International Conference on Multimedia Retrieval (ICMR) 2013 and the Best Student Paper Award from the International Conference on Multimedia Modeling (MMM) 2016.



Qixiang Geng received the BS degree in Computer Science and Technology at Nanjing Audit University in 2019. He is now a master student with the College of Computer Science and Technology, Nanjing University of Aeronautics and Astronautics. His research interests include computer vision, especially in object detection. He is currently a research intern with Senstime.



Mingqiang Wei received his Ph.D degree (2014) in Computer Science and Engineering from the Chinese University of Hong Kong (CUHK). He is a professor at the School of Computer Science and Technology, Nanjing University of Aeronautics and Astronautics (NUAA). Before joining NUAA, he served as an assistant professor at Hefei University of Technology, and a postdoctoral fellow at CUHK. He was a recipient of the CUHK Young Scholar Thesis Awards in 2014. He is now an Associate Editor for the Visual Computer Journal, Journal of Electronic Imaging, Journal of Image and Graphics. His research interests focus on 3D vision, computer graphics, and deep learning.



Huiyu Zhou received a Bachelor of Engineering degree in Radio Technology from Huazhong University of Science and Technology of China (1990), and a Master of Science degree in Biomedical Engineering from University of Dundee of United Kingdom (2002), respectively. He was awarded a Doctor of Philosophy degree in Computer Vision from Heriot-Watt University, Edinburgh, United Kingdom (2006). Dr. Zhou currently is a full Professor at School of Informatics, University of Leicester, United Kingdom. He has published over 350 peer-reviewed papers in the field.